JOURNAL OF MATERIALS SCIENCE: MATERIALS IN MEDICINE **16** (2005) 467–475

Microporosity enhances bioactivity of synthetic bone graft substitutes

K. A. HING[1,*], B. ANNAZ[1], S. SAEED[2], P. A. REVELL[2], T. BUCKLAND[3]
[1]*IRC in Biomedical Materials, Queen Mary University of London, London, E1 4NS, UK*
E-mail: k.a.hing@qmul.ac.uk
[2]*Osteoarticular Research Group, University College London, Royal Free Campus, London, NW3 2PF, UK*
[3]*ApaTech Ltd., IRC in Biomedical Materials, Queen Mary University of London, London, E1 4NS, UK*

This paper describes an investigation into the influence of microporosity on early osseointegration and final bone volume within porous hydroxyapatite (HA) bone graft substitutes (BGS). Four paired grades of BGS were studied, two (HA70-1 and HA70-2) with a nominal total porosity of 70% and two (HA80-1 and HA80-2) with a total-porosity of 80%. Within each of the total-porosity paired grades the nominal volume fraction of microporosity within the HA struts was varied such that the strut porosity of HA70-1 and HA80-1 was 10% while the strut-porosity of HA70-2 and HA80-2 was 20%. Cylindrical specimens, 4.5 mm diameter $\times$ 6.5 mm length, were implanted in the femoral condyle of 6 month New Zealand White rabbits and retrieved for histological, histomorphometric, and mechanical analysis at 1, 3, 12 and 24 weeks. Histological observations demonstrated variation in the degree of capillary penetration at 1 week and bone morphology within scaffolds 3–24 weeks. Moreover, histomorphometry demonstrated a significant increase in bone volume within 20% strut-porosity scaffolds at 3 weeks and that the mineral apposition rate within these scaffolds over the 1–2 week period was significantly higher. However, an elevated level of bone volume was only maintained at 24 weeks in HA80-2 and there was no significant difference in bone volume at either 12 or 24 weeks for 70% total-porosity scaffolds. The results of mechanical testing suggested that this disparity in behaviour between 70 and 80% total-porosity scaffolds may have reflected variations in scaffold mechanics and the degree of reinforcement conferred to the bone-BGS composite once fully integrated. Together these results indicate that manipulation of the levels of microporosity within a BGS can be used to accelerate osseointegration and elevate the equilibrium volume of bone.

1. Introduction

Demographic trends and greater expectations regarding quality of life have resulted in an increasing global demand for orthopaedic implants to replace or repair damaged bones & joints [1]. In bone augmentation, auto-grafting is the current 'gold standard' where bone, containing live cells and growth factors, is harvested from the patient. However, autografting has its limitations, the principle ones being the requirement for a second surgical site with associated donor site pain and morbidity, in addition to the obvious limitations in supply. Alternatively allografts (donor bone obtained from a bone bank) are used, however after sterilisation treatments these do not contain the biologic factors and have impaired strength, furthermore supply and bone quality cannot be guaranteed. Porous ceramics have been considered for use as synthetic bone graft substitutes for over 30 years [2], with many reports of a greater degree and faster rate of bone penetration with increasing macroporosity (i.e. pores >50 μm in size) in a wide variety of BGS [3–7]. This phenomenon has been related to both the greater volume available for in-growth and the openness or interconnectivity of the structure. Bone is a mineralised tissue that relies heavily on the presence of an internal blood supply. Any new bone formation or repair must always be preceded by the formation of a vascular network, the rapidity and extent of which is strongly influenced by the degree of structural interconnectivity between pores [8]. This has been elegantly demonstrated by a greater penetration of bone in porous

*Author to whom all correspondence should be addressed.

implants with larger pore interconnection sizes [7, 9] and improved integration within porous constructs with smaller but well connected porosity as compared to constructs with larger more isolated pores [3].

Furthermore, it is well known that bone is functionally adaptive, i.e. that it responds to external mechanical stimuli to either reduce or increase its mass as required [10]. Mechanical stimuli regulate many cell types, including osteoblasts and osteocytes [11], moreover they have recently been shown to mediate osteoblastic differentiation of osteoprogenitor cells [12]. Therefore, it is possible to see how variation of local strain in scaffold struts as a result of porosity variation may induce or inhibit bone formation. Thus the degree of scaffold porosity could be responsible for regulating the bioactivity of a BGS as a function of its influence on structural permeability [3] (so controlling initial rate of osseointegration) and the local mechanical environment (so mediating the equilibrium volume of new bone within the repair site [4]). However, while it is recognised that both the rate of integration & the volume of regenerated bone may be dependent on features of the macroporosity, recent studies *in vitro* & *in vivo* have demonstrated biological sensitivity to the level of microporosity within the ceramic struts [13–16]. With evidence to suggest that initially this is through a combination of enhanced angiogenesis [15] and cell adhesion [13, 14], while in the longer term the influence of both micro and macro-porosity on bone adaptation appears to play a role [4, 16].

The aim of this study was to investigate the influence of controlled variations in levels of strut porosity on osseointegration within porous HA (PHA) scaffolds with varied levels of total porosity in order to explore any influence on the rate of early bone formation and the final volume of regenerated bone within the defect site.

2. Materials and methods

Phase pure porous hydroxyapatite (PHA) scaffolds were produced using a novel slip foaming technique which enabled independent control of the level of total porosity and the level of strut porosity [17, 18], where strut porosity is the percentage of microporosity as a fraction of the strut volume, (Fig. 1). Two grades HA70-1 and HA70-2 were prepared with a nominal total-porosity of 70% while a further two grades, HA80-1 and HA80-2 were prepared with a nominal total-porosity of 80% (Fig. 2(a)). Within each of the total-porosity paired grades the nominal volume fraction of microporosity within the HA struts was varied such that the strut-porosity of HA70-1 and HA80-1 was 10% while the strut-porosity of HA70-2 and HA80-2 was 20% (Fig. 2(b)). Phase purity post sintering was verified using X-ray diffractometry (Fig. 3), performed on a Siemens D-5000 X-ray diffractometer in flat plate geometry with Cu-K_α radiation and the X-ray generator operated at 40 kV and 40 mA. Data were acquired from 25–40° 2θ, with a step size of 0.02° at 2.5 s per step and identification of the phases present was achieved by comparing the obtained diffraction patterns with International centre for diffraction data (ICDD) powder diffraction file (PDF) cards [19].

Quantification of both the macro- and microporosity was performed through a combination of immersion densitometry and image analysis of strut porosity from serial sections [20] using a Zeiss Axioskop optical microscope linked to a KS300 image analyser. Immersion densitometry was performed using water on 5 specimens from each batch, each analysed in triplicate. Image analysis was performed on 6 images of 2–3 sections taken from an embedded specimen from each batch. Approximately 10 mm cube specimens were prepared for immersion densitometry and care was taken to remove any surface skin. A minimum size of 15 mm square was used for characterisation of porosity by image analysis, the specimens were vacuum embedded in Epofix resin (Struers, Glasgow) and left to cure at room temperature overnight. Once cured the specimens were polished on an Abramin automatic polisher (Struers, Glasgow) to a 0.04 μm surface finish.

Cylindrical specimens 4.5 mm in diameter & 6.5 mm long were implanted in the cranial, or from an anthropomorphic perspective, 'distal' end of the femur (Fig. 4) of 6 month old New Zealand White rabbits [4] & retrieved for histological, histomorphometric and/or mechanical analysis at 1, 3, 12 and 24 weeks. Specimens for histological/histomorphometric analysis were

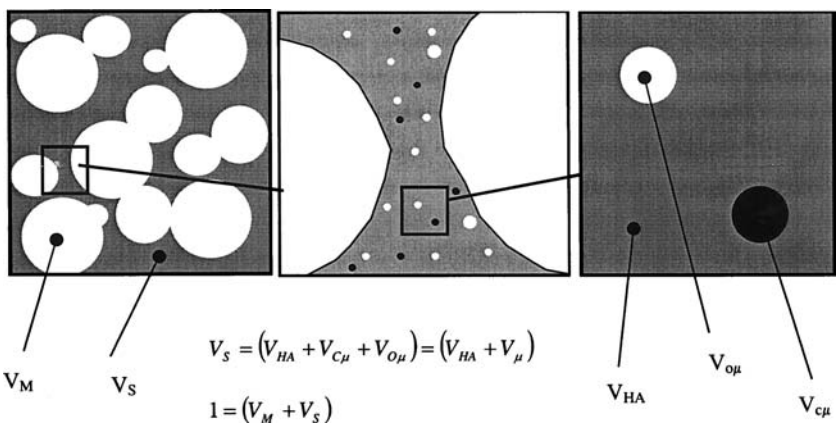

Figure 1 Schematic diagram of the different HA and porosity volume fractions within a porous HA scaffold, where V_S = the total strut volume fraction, V_M = the total macropore volume fraction, $V_{C\mu}$ = the closed micropore volume fraction, V_{HA} = the total HA volume fraction and $V_{O\mu}$ = the open micropore volume fraction.

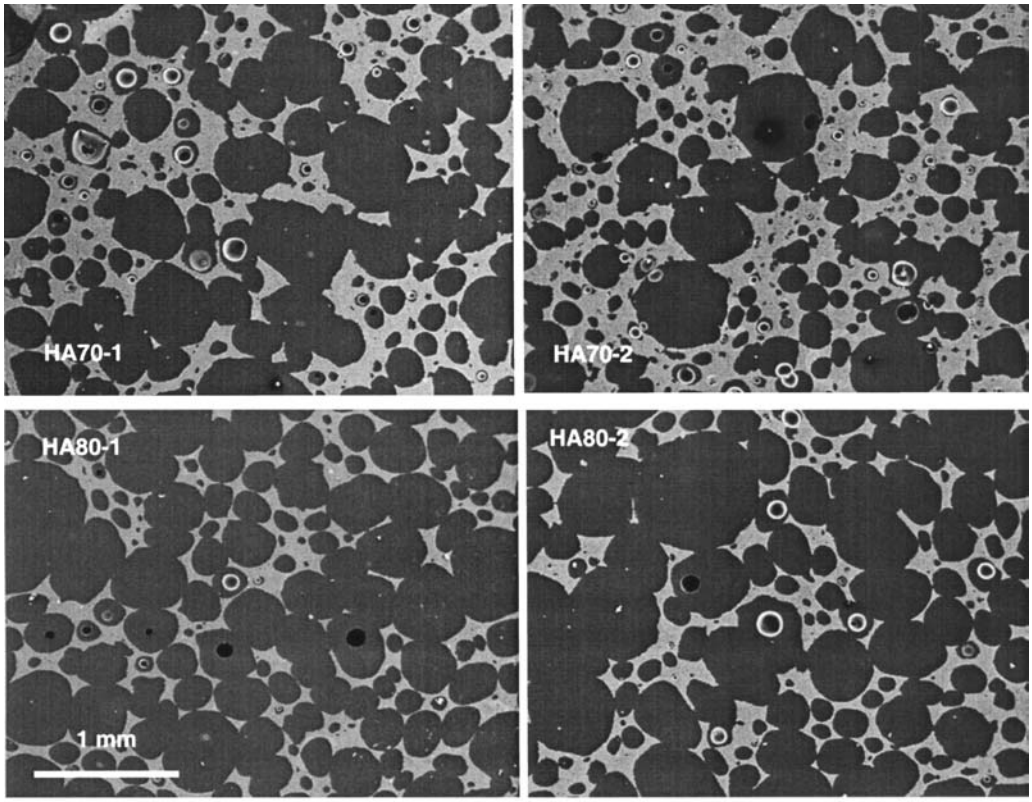

Figure 2 (a) Macropore structures of the four scaffold grades and (b) Microporosity structures of the four scaffold grades.

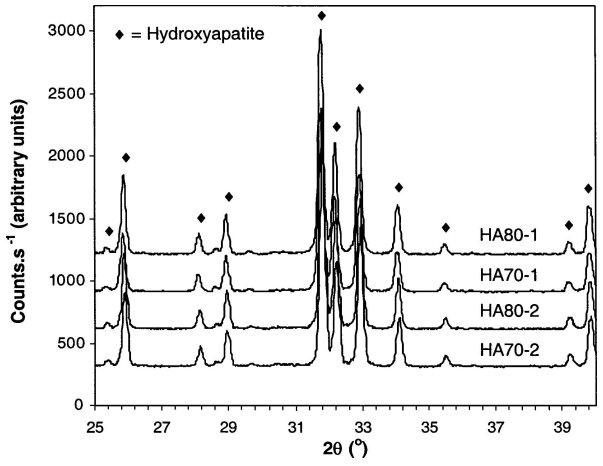

Figure 3 XRD patterns for the four scaffold grades.

trimmed and placed immediately in formal alcohol fixative (comprising 70% ethanol) for a period of at least 4 days. Fixed tissues were dehydrated and embedded in Technovit resin. The resin blocks were then sectioned in the sagittal plane (Fig. 4) and processed through to semi-thin (5–10 μm) section using the Exakt technique [21]. At least three sections were obtained from each implant; one was left unstained for fluorescence microscopy while the others were stained with either toluidine blue or Goldner's trichrome. Histomorphometry was performed using point counting techniques [22] where the space occupied by bone and HA within each implantation site was measured in order to determine the total volumes occupied by bone ingrowth, implant and porosity for each specimen, so enabling calculation of both the absolute and normalised volume% of new bone [4, 23]. The mineral apposition rate (MAR) was determined through administration of fluorochrome labels at 1 & 2 weeks post op to animals allocated to the three week survival group [24]. In order to aid histological and histomophometric examination five regional analysis zones were defined within the implants, and the progression of events such as angiogenesis and new bone formation monitored within these zones (Fig. 4).

Compression testing of both as received cylindrical specimens ($n_{\text{per grade}} = 10$), non-operated control bone

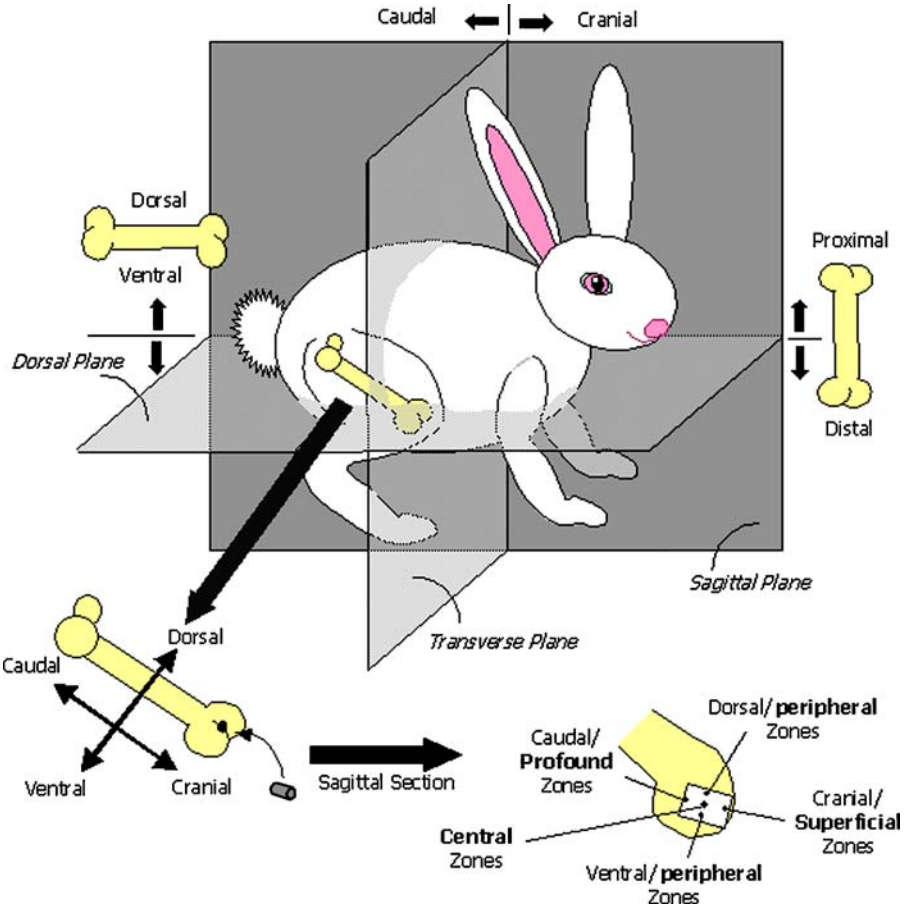

Figure 4 Schematic diagram indicating implantation site and location of analysis zones within a histological section.

($n = 10$) and retrieved implants ($n_{\text{per grade}} = 5$) was performed using an Instron 4464 bench-top test machine, fitted with a 2 kN load cell, using test templates created on Series IX Automated Testing System 1.26 (Instron, High Wycombe, England). Retrieved implants were tested in an environmental chamber at 37 °C. An axial pre-load of 0.005 kN was applied with a crosshead velocity of 0.05 mm s^{-1} prior to application of load to failure with a crosshead velocity of 0.001 mm·s^{-1}. The test was recorded electronically with a sample rate of 0.5 points·s^{-1}[4, 23].

3. Results

Characterisation of the porosity demonstrated that there was no significant difference in either the macroporosity volume fraction or the total porosity of the paired 70 & 80% total-porosity grades (Fig. 5(a)). Furthermore, over 85% of the strut-porosity present within all grades was open & interconnected and was found to vary significantly ($P < 0.05$) between the high and low strut porosity grade paired groups (Fig. 5(b)).

Histological analysis at one week demonstrated that bone ingrowth was of a predominantly woven nature (Fig. 6), and that the primary direction of integration was from the profound zones through to the central zones with some ingress from the peripheral zones. The degree of bone penetration varied with both total-porosity and strut-porosity, within HA80-2, HA80-1 and HA70-2 scaffolds it had reached a depth of 1.0,

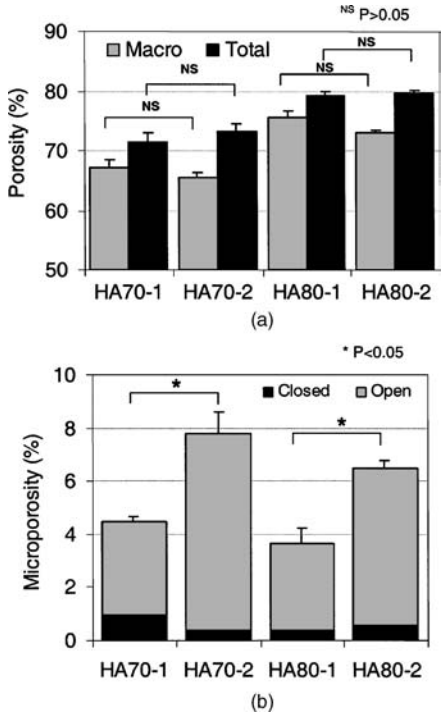

Figure 5 (a) Total and macro- porosity variation within the four scaffold grades and (b) Open and closed microporosity variation within the four scaffold grades.

1.0–0.5 and 0.5 mm from the profound end, respectively, whereas in HA70-1 scaffolds it was limited to just within the profound & peripheral porosity. Neovascularisation was evident throughout HA80-2, in the central and profound-central porosity of HA70-2 &

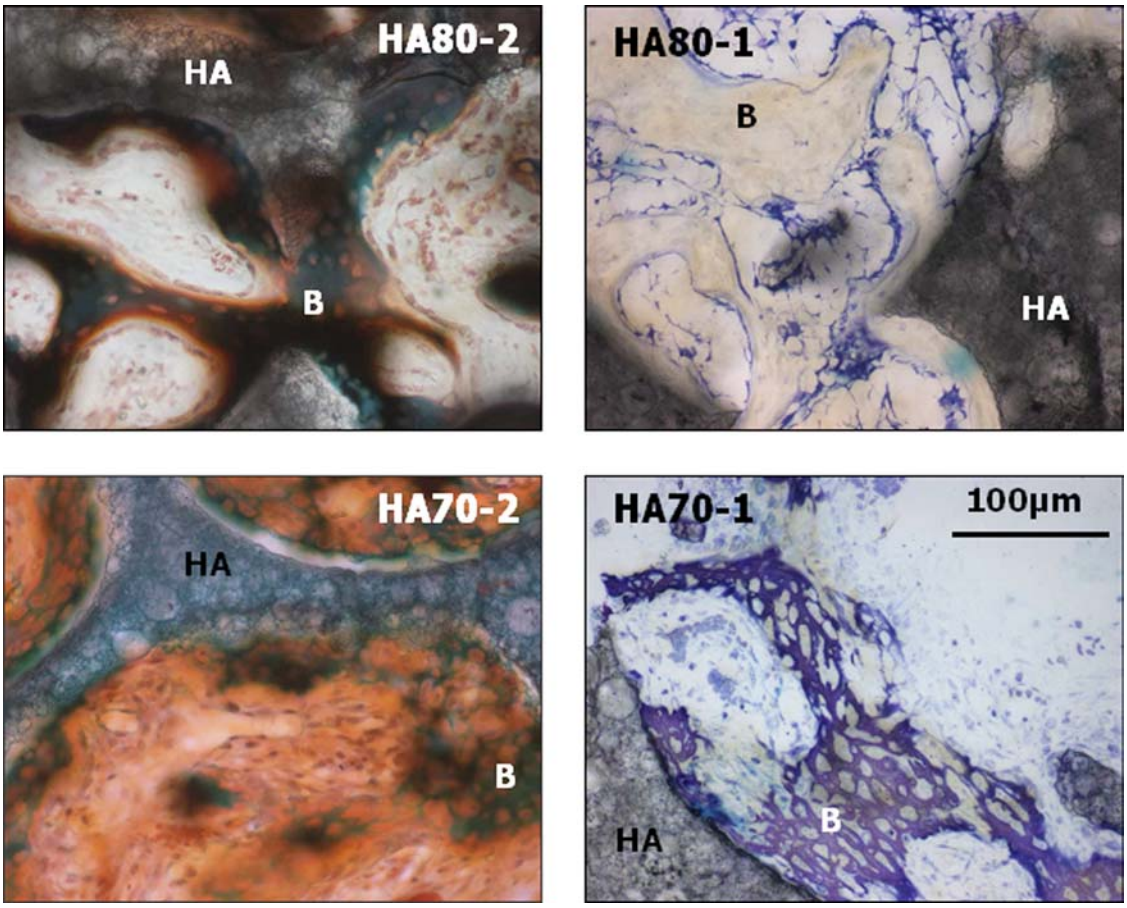

Figure 6 Variation in the morphology of bone found within the 70 and 80% total-porosity paired high and low microporosity BGS scaffolds after 1 week *in vivo*. (HA = BGS strut, B = new bone, HA80-2 & HA70-2 Goldners Trichrome, HA80-1 & HA70-1 Toluidine blue).

HA80-1 respectively, but limited to the profound & peripheral porosity of HA70-1 (Fig. 7). At 3 weeks all new bone was almost exclusively lamellar, however the morphology of bone ingrowth varied with both strut-porosity and total-porosity, appearing denser, i.e. having thicker trabeculae, within the higher microporosity grades, HA70-2 & HA80-2, while ingrowth within the higher total-porosity grades, HA80-1 and HA80-2, was characterised by bone 'islands' in the centre of pores indicative of bone spanning trabeculae, whereas bone within HA70-1 and HA70-2 scaffolds tended to be associated with pore surfaces (Fig. 8). Bone penetration extended throughout the central zones of all scaffolds, with some ingrowth within the superficial zones of HA80-2 scaffolds and limited apposition within the superficial zones of HA70-2 scaffolds. Capillaries were observed throughout HA80-2 and had penetrated to central-superficial zones in HA70-2 and HA80-1 and central zones in HA70-1. There were active regions of bone apposition and resorption (remodelling) through out the profound and central zones of all BGS. By 12 weeks the vascular network was well established in all BGS, marrow had penetrated through out the central zones and the bone had a more mature, organised, lamellar structure however the bone morphology continued to vary within the different porosity BGS, although at this time point the delineation appeared to be between HA80-2 and all other BGS. In HA80-2 bone was characterised by thick pore coverage in combination with trabeculae that spanned pores. There was no significant variation in ingrowth density through out the defect site. Within the other porosity BGS bone morphology varied with location in the defect site, being generally denser in the superficial zone and at anchor points at peripheral porosity. Bone surfaces were often occupied by active osteoblasts or had a scalloped morphology suggestive of regions of active remodelling, particularly in low microporosity BGS (Fig. 9). At 24 weeks there was no significant change in the distribution of bone noted at 12 weeks within the various BGS. The only notable change was in the level of cellular activity, at 24 weeks this was much reduced with few active regions of bone apposition/resorption outside the central zones.

At 3 weeks, despite having similar porosity, there was a significant difference in the absolute % bone ingrowth (%AB) between the total-porosity paired grades of PHA ($^{*}P < 0.05$, Fig. 10(a)) & in the mineral apposition rate (MAR) of bone deposited between weeks 1 & 2 ($^{**}P < 0.005$, Fig. 11). Furthermore, an increase in total-porosity of scaffolds with a strut-porosity of 10% did not significantly affect the volume of ingrowth when normalised for the available pore space (%NB) or the MAR (HA70-1 vs HA80-1 Figs. 10(b) and 11), whereas at 20% strut-porosity there was a significant improvement in both %NB values and MAR with an increase in total-porosity (HA70-2 vs HA80-2 $^{*}P < 0.05$ Figs. 10(b) and 11). In contrast at 12 weeks there were no significant differences in either of the total-porosity paired grades, although the magnitude of bone

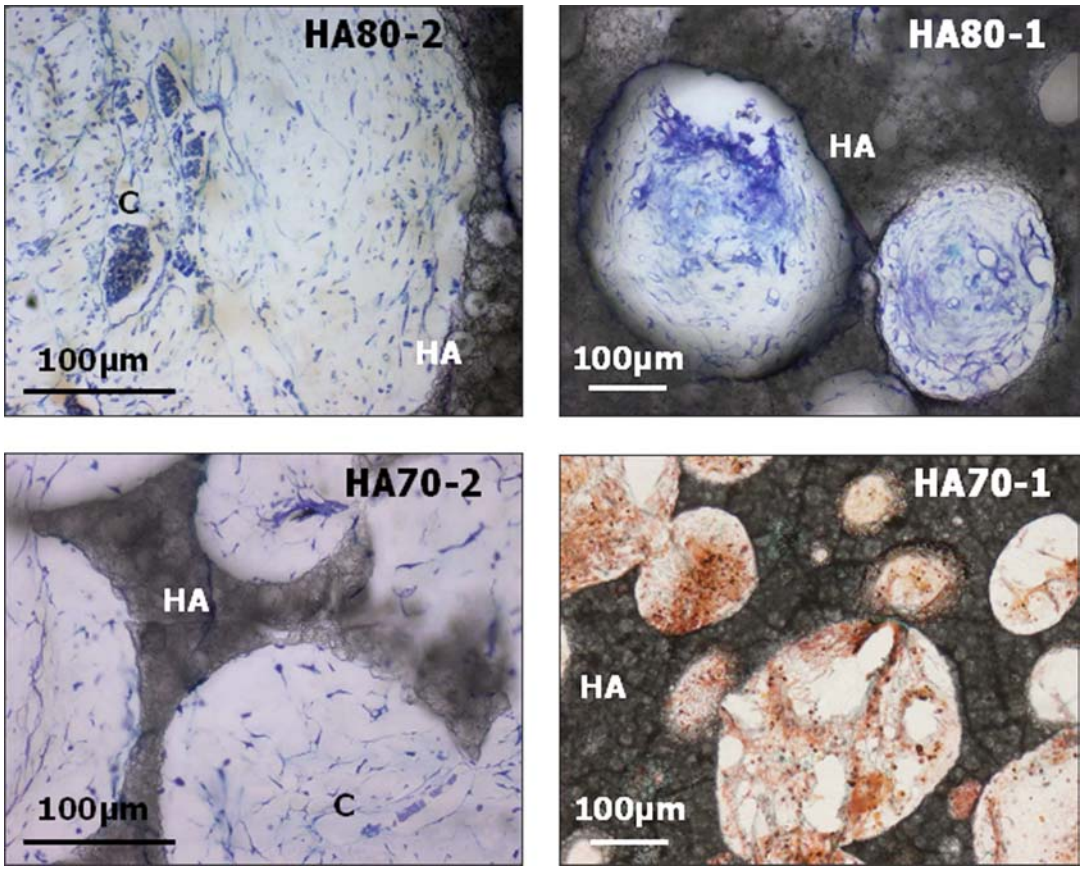

Figure 7 Variation in capillary formation within the central porosity of the 70 and 80% total-porosity paired high and low microporosity BGS scaffolds after 1 week *in vivo*. (HA = BGS strut, C = capillary, HA80-2 & HA70-2 Goldners Trichrome, HA80-1 & HA70-1 Toluidine blue).

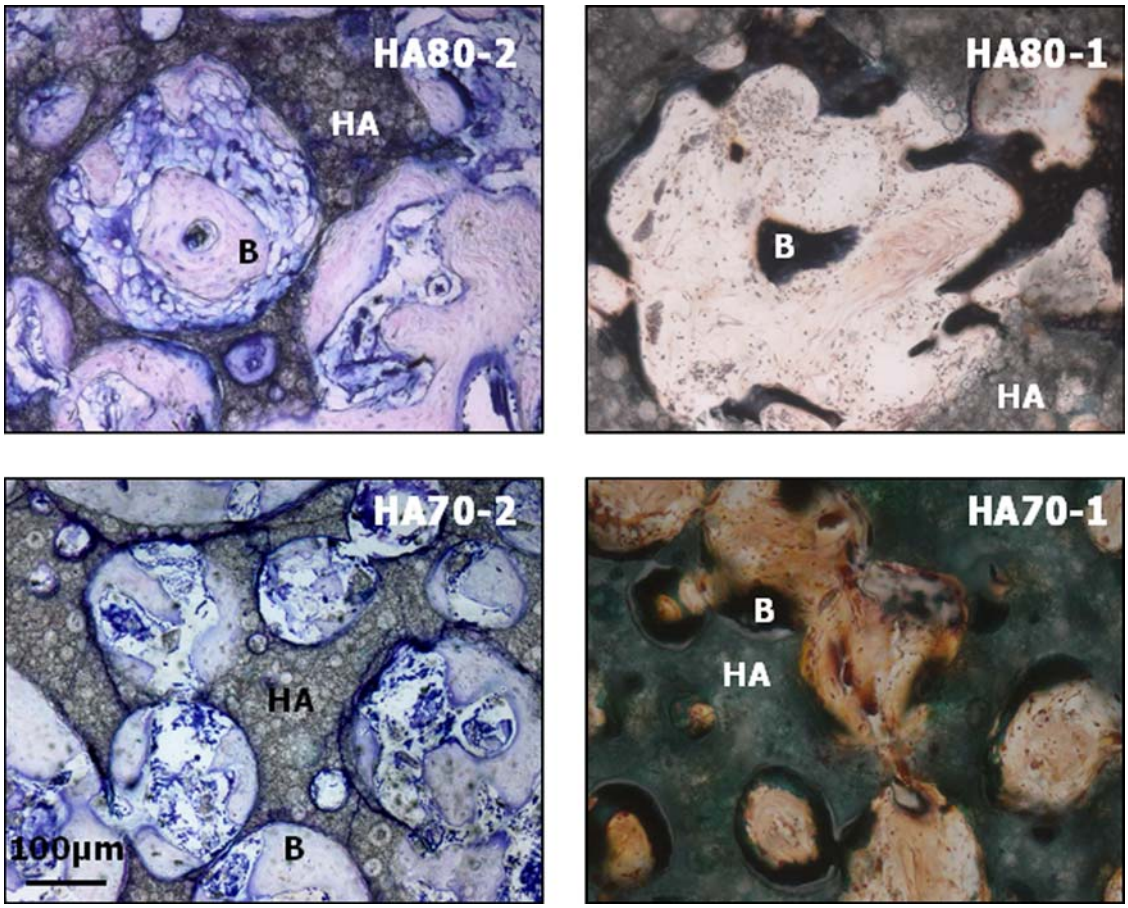

Figure 8 Variation in the morphology of bone found within the central porosity of 70 and 80% total-porosity paired high and low microporosity BGS scaffolds after 3 weeks *in vivo*. (HA = BGS strut, B = bone ingrowth. HA80-2 & HA70-2 Toluidine blue, HA80-1 & HA70-1 Goldners Trichrome).

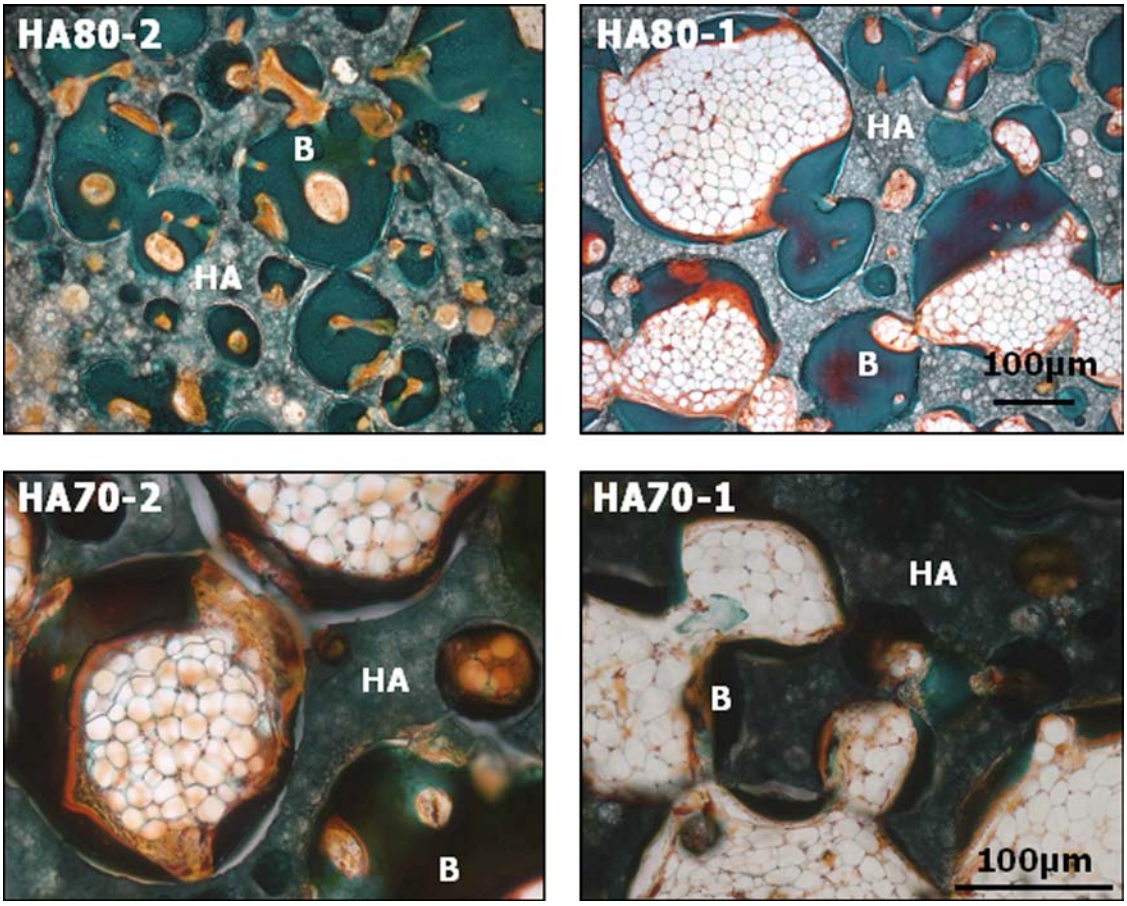

Figure 9 Variation in the morphology of bone found within the central porosity of 70 and 80% total-porosity paired high and low microporosity BGS scaffolds after 12 weeks *in vivo*. (HA = BGS strut, B = bone ingrowth. All Goldners Trichrome).

volume was consistently higher in the high microporosity grades (HA70-2, HA80-2 Fig. 10). By 24 weeks both the %AB and %NB was significantly greater in HA80-2 as compared to HA80-1. In contrast the magnitude of ingrowth in the paired 70% total-porosity BGS was identical. Moreover, the %AB of HA70-1, HA70-2 and HA80-1 was statistically similar despite HA80-1 having a 10% increase in total porosity (Fig. 10).

Prior to implantation the ultimate compressive strengths (UCS) of the as-received BGS varied significantly across the total-porosity paired grades (i.e. HA70-1 vs HA70-2, $P < 0.01$ and HA80-1 vs HA80-2, $P < 0.05$ Fig. 12). However, mechanical testing of the retrieved implants at both 3 and 24 weeks demonstrated the significant reinforcing effect of integration with new bone that resulted in a 300–400% increase in UCS in just 3 weeks (Fig. 12). There was no variation in UCS across total-porosity paired grades at either 3 or 24 weeks, moreover at 24 weeks there was no significant difference in UCS across the entire group of BGS. At 3 weeks the UCS of HA70-1 was significantly greater than that of both 80% total-porosity grades ($P < 0.005$).

4. Discussion

These results indicate that, in PHA scaffolds with equivalent levels of total-porosity, the presence of microporosity altered the pattern and dynamics of osseointegration, where BGS with increased levels of microporosity promoted the apposition of greater volumes of new bone in a more dense morphology at earlier time points. This effect appears to be tied to the rate of vascularisation within the scaffolds, where the disparity in capillary penetration at early time points suggests that the rate of development of the vascular network is linked to the strut porosity variation. Mechanistically, this could be attributed to either increased permeability within the microporous scaffolds enhancing nutrient transfer, leading to faster bone apposition and/or angiogenesis, or it may result from the greater degree of microporosity providing either a larger surface area or a geometrically more suitable substrate for angiogenic and/or osteogenic protein adsorption & cell anchorage, leading to the more rapid induction of angiogenesis and thus bone apposition. This latter hypothesis is supported by previous studies of angiogenesis and osteoblast response *in vivo* and *in vitro*, respectively. Immunohistochemical localisation demonstrated association of VEGF with the HA surface in addition to a close relationship between the HA surface and newly formed capillaries [25] *in vivo*, while an affinity was observed between the fidopillia of primary human osteoblasts-like cells and micropores [13] *in vitro*, respectively.

However, the variation in MAR over the 1–2 week period across the different porosity BGS, would suggest that the alteration in the pattern of osseointegration transpired through a direct increase in the rate of bone formation, suggesting the promotion of early rapid woven bone formation in the more permeable microporous

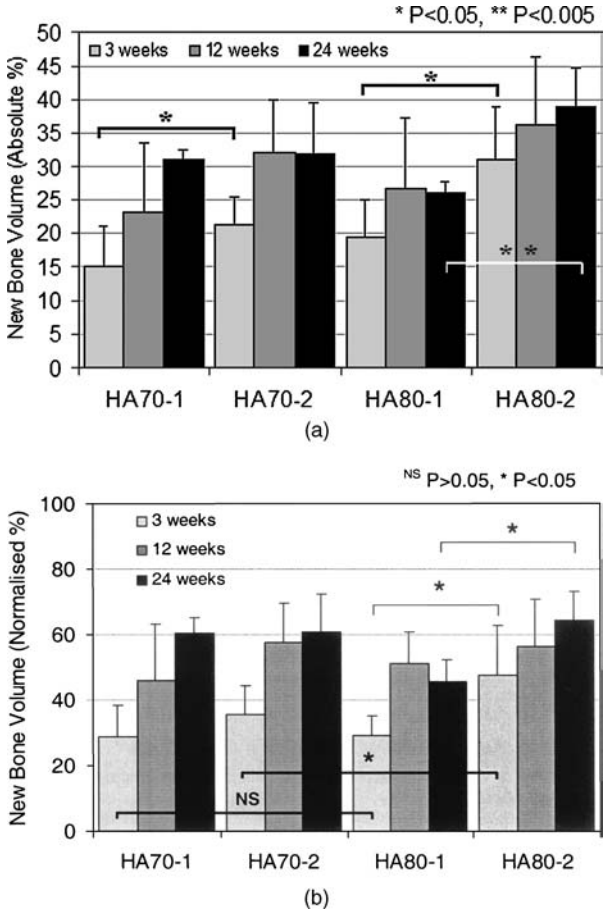

Figure 10 (a) Variation in absolute volume of new bone within the four scaffold grades and (b) Variation in normalised volume of new bone within the four scaffold grades.

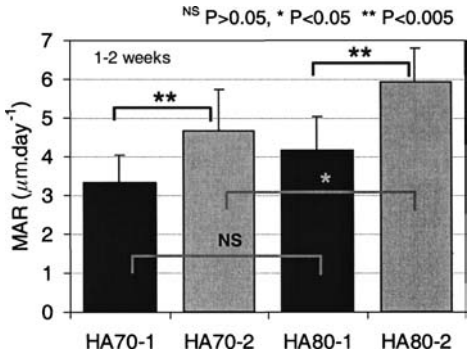

Figure 11 Variation in mineral apposition rate (MAR) of bone between weeks 1-2 within the four scaffold grades.

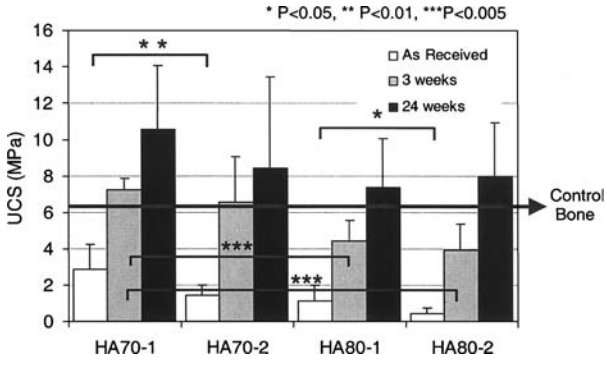

Figure 12 Variation in ultimate compressive strength (UCS) of the four scaffold grades before implantation and after 3 and 24 weeks *in vivo*.

scaffolds (which may not necessarily be linked to the rate of angiogenesis). However, no difference was observed in the organisational maturity of the labelled bone across the four porosity grades, moreover a significant portion of the bone labelled at both 1 and 2 weeks was lamellar. Woven bone, where it occurred, tended to be found largely within the peripheral zones. Taken with the histological observations of predominantly woven bone formation in 1 week survival sections, this predominance of lamellar bone formation from 1–2 weeks would suggest that rapid woven apposition was limited to the periphery during fixation of the implant, with more ordered bone formation dominating after stabilisation of the wound site. Thus the similarity in organisational maturity of bone within the porosity would suggest that the variation in rate within the scaffolds did not correlate to switching between predominantly lamellar or woven modes of bone formation within regions of the scaffold as vascular penetration progressed, but that beyond the first week post-implantation and establishment of graft fixation, the scaffolds supported the direct apposition of lamellar bone, the rate of formation of which was tied to the local conditions of oxygenation and/or the concentration of osteogenic factors at the graft surface. A more detailed examination of the dynamics of apposition in the 2–6 week period will be necessary to identify whether this alteration in the rate of bone formation reflects a gross acceleration of lamellar mineral apposition rate in more microporous scaffolds or whether the increase in microporosity has lead to faster angiogenesis and a temporal shift in the healing cascade.

The alteration in the early pattern of osseointegration and variation in apposition rate only resulted in a significant difference in bone volume between both the 70 and 80% total porosity paired grades at 3 weeks. Furthermore, ultimate levels of bone volume were only significantly different at 24 weeks between HA80-1 and HA80-2. Thus a 10% increase in total porosity had no significant effect on final bone volume for low microporosity BGS (i.e. between HA70-1 and HA80-1). This implies that increasing the microporosity had an additive affect on the absolute equilibrium level of bone established within the macroporosity.

Measurement of the UCS of retrieved implants at 3 weeks demonstrated the extent of reinforcement conferred to the BGS by the new bone, even when partially integrated. Of note was the lack of significant variation in UCS between the total-porosity paired grades, especially given the significant variation in their bone volumes at this time point. Moreover, at 24 weeks there was no significant difference in the UCS of the retrieved implants irrespective of their original porosity and hence strength, again despite the significantly greater level of ingrowth in HA80-2. Taken together with the variation in bone morphology within the four grades of BGS at 12 and 24 weeks (where bone ingrowth remains uniformly dense throughout HA80-2, but varies with location in the other grades) the uniformity in UCS at 24 weeks implies that both bone volume and morphology within BGS may be mechanically mediated at later time points. This phenomenon of bone adaptation within PHA has

previously been reported [4, 16], moreover, remodelling within normal bone is believed to be in response to micro-fractures and changes in the mechanical environment occurring within the bone [26–28]. Thus it is likely that the reduction in scaffold modulus associated with increasing the strut porosity in HA80-20 scaffolds shifted the strut modulus below a threshold value resulting in a swing in the equilibrium local bone cell activity towards a greater degree of stable bone apposition. Interestingly, the absolute equilibrium level of bone established within the macroporosity of HA70-1 was statistically similar to that within HA70-2 and HA80-1 at 24 weeks, suggesting that in order to attain a significant reduction in the equilibrium level of bone the scaffold modulus may require increasing beyond a further threshold value than that of HA70-1. Moreover, once integrated none of the implants were significantly different to control bone from the same site retrieved and tested under identical conditions.

5. Conclusions

The distribution of porosity volume between the macro- and micro- structure had a significant effect on the early pattern and dynamics of osseointegration, possibly though its influence on permeability and angiogenesis, where an increase in either total- or strut-porosity accelerated osseointegration.

In the longer term the dominating factor was the influence of strut-porosity on the mechanics of the scaffold, where the variation in bone ingrowth coupled with the consistency in UCS across the BGS grades at 24 weeks supported the hypothesis that mechano–transduction was the dominant mechanism controlling ultimate bone volume and morphology. This phenomenon resulted in scaffolds with a significantly lower level of total porosity (HA70-2 & HA70-1) having an equivalent level of ultimate bone volume as the 'more porous' HA80-1.

Acknowledgments

The authors would like to thank Tom MacInnes, and Katherina Guth for their technical expertise. This work was supported in part by EPSRC grant No. AF/99/0077 & by ApaTech Ltd., UK.

References

1. Clinica Reports 2002, Orthopaedics:Key markets & emerging technologies, CBS905E.
2. J. J. KLAWITTER and S. F. HULBERT, *J. Biomed Mater. Res.* **5** (1971) 161.
3. P. S. EGGLI, W. MULLER and R. K. SCHENK, *Clin. Orthop. Relat. Res.* **232** (1988) 127.
4. K. A. HING, S. M. BEST, K. E. TANNER, W. BONFIELD and P. A. REVELL, *J. Biomed. Mater. Res.* **68A** (2004) 187.
5. R. E HOLMES, V. MOONEY, R. BUCHOLZ and A. TENCER, *Clin. Orthop. Rel. Res.* **188** (1984) 252.
6. J. J. KLAWITTER, J. G. BAGWELL, A. M. WEINSTEIN, B. W. SAUER and J. R. PRUITT, *J. Biomed. Mater. Res.* **10** (1976) 311.
7. J. H. KÜHNE, R. BARTL, B. FRISH, C. HANMER, V. JANSSON and M. ZIMMER, *Acta Orthop. Scand.* **65**(3) (1994) 246.
8. P. A. RUBIN, J. K. POPHAM, J. R. BILYK and J. W. SHORE, *Ophthal. Plast. Reconstr. Surg.* **10**(2) (1994) 96.
9. K. L. KILPADI, A. A. SAWYER, C. W. PRINCE, P. L. CHANG and S. L. BELLIS, *J. Biomed. Mater. Res.* **68A**(2) (2004) 273.
10. J. WOLFF, *Virchows Arch. Path. Anat. Physiol.* **50** (1870).
11. H. M. FROST, *Anat. Rec.* **219**(1) (1987) 1.
12. J. R. MAUNEY, S. SJOSTORM, J. BLUMBERG, R. HORAN, J. P. O'LEARY, G. VUNJAK-NOVAKOVIC, V. VOLLOCH and D. L. KAPLAN, *Calcif. Tissue. Int.* **74**(5) (2004) 458.
13. B. ANNAZ, K. A. HING, M. V. KAYSER, T. BUCKLAND and L. DI SILVIO, *J. Microscopy.* **215**(1) (2004) 100.
14. A. BIGNON, J. CHOUTEAU, J. CHEVALIER, G. FANTOZZI, J. P. CARRET, P. CHAVASSIEUX, G. BOIVIN, M. MELIN and D. HARTMANN, *J. Mater. Sci. Mater. Med.* **14**(3) (2003)1089.
15. K. A. HING, S. SAEED, B. ANNAZ, T. BUCKLAND and P. A. REVELL, *Key Engng. Mater.* **254–256** (2004) 273.
16. A. BOYDE, A. CORSI, R. QUARTO, R. CANCEDDA and P. BIANCO, *Bone* **24**(6) (1999) 579.
17. K. A. HING and W. BONFIELD, Foamed Ceramics, International Patent No. GB99/03283. (1999)
18. K. A. HING and T. BUCKLAND, Ceramic Biomaterial, UK Patent application No. 03258.33.2 (2003).
19. Powder diffraction file (PDF) 9-432, International centre for diffraction data, Newton Square Pensilvania USA
20. K. A. HING, S. M. BEST and W. BONFIELD, *J. Mater. Sci. Mater. Med.* **10**(3) (1999) 135.
21. K. DONATH, *J. Oral. Pathology* **11** (1982) 318.
22. E. R. WEIBEL and H. E. ELIAS, in "Quantitative Methods in Morphology" (Springer-Verlag, Berlin 1967) p. 87.
23. K. A. HING, S. M. BEST, P. A. REVELL, K. E. TANNER and W. BONFIELD, *Proc. Instn. Mech. Engrs. Part. H* **212** (1998) 437.
24. H. M. FROST in "Bone Histomorphometry" edited by P.J. Meunier (1976) p. 361.
25. S. OHTSUBO, M. MATSUDA and M. TAKEKAWA, *Histol Histopathol.* **18**(1) (2003) 153.
26. J. A. O'CONNOR, L. E. LANYON and J. H. MACFIE, *J. Biomech.* **15** (1982) 767.
27. L. E. LANYON, A. E. GOODSHIP, C. J. PIE and J. H, *ibid.* **15**(3) (1982) 141.
28. D. B. BURR, R. B. MARTIN, M. B. SCHAFFLER and E. L. RADIN, *ibid.* **18** (1985)189.

Received 1 July
and accepted 1 November 2004